Air Data Sensor Fault Detection and Diagnosis in the Presence of Atmospheric Turbulence

Theory and Experimental Validation with Real Flight Data

Lu, Peng; Van Kampen, Erik Jan; De Visser, Coen; Chu, Qiping

DOI
10.1109/TCST.2020.3025725

Publication date
2021

Document Version
Final published version

Published in
IEEE Transactions on Control Systems Technology

Citation (APA)
Lu, P., Van Kampen, E. J., De Visser, C., & Chu, Q. (2021). Air Data Sensor Fault Detection and Diagnosis in the Presence of Atmospheric Turbulence: Theory and Experimental Validation with Real Flight Data. *IEEE Transactions on Control Systems Technology*, *29*(5), 2255-2263. Article 9211802. https://doi.org/10.1109/TCST.2020.3025725

Air Data Sensor Fault Detection and Diagnosis in the Presence of Atmospheric Turbulence: Theory and Experimental Validation With Real Flight Data

Peng Lu, *Member, IEEE*, Erik-Jan van Kampen, *Member, IEEE*, Coen de Visser, *Member, IEEE*, and Qiping Chu

***Abstract*— Managing air data sensor fault detection and diagnosis (FDD) in the presence of atmospheric turbulence is challenging since the effects of faults and turbulence are coupled. Existing FDD approaches cannot decouple the faults from the turbulence. To address this challenge, this brief first proposes a novel kinematic model that incorporates the effects of the turbulence. This model is valid inside the entire flight envelope, and there is no need to design a linear parameter varying system. Then, the double-model adaptive estimation algorithm is extended to achieve unbiased state estimation even in the presence of unknown disturbances. The proposed approach is validated using generated turbulence data with various scale lengths and intensities. More importantly, the proposed approach is successfully validated using the real flight test data of a business jet when it is experiencing atmospheric turbulence.**

***Index Terms*— Air data sensor (ADS) fault detection, atmospheric turbulence, disturbances, double-model adaptive estimation (DMAE), fault detection and diagnosis (FDD), real flight data.**

I. Introduction

AIR data sensor (ADS) faults have a significant effect on aircraft safety. ADSs are installed outside the fuselage and can readily be affected by weather conditions. ADS faults can result in fatal accidents, such as the Airbus A330 flight AF 447 [1] and the B2 bomber [2]. Moreover, these sensor faults can also inappropriately trigger emergency systems onboard the aircraft, such as the maneuvering characteristics augmentation system on the Boeing 737 MAX, which led to fatal accidents. To increase aircraft safety, ADS faults must be detected and diagnosed in time.

ADS faults have been addressed by a number of studies [3]–[7]. Earlier methods mainly replace the ADS with other systems, such as a flush air data system [8] and a virtual air data system [9]. Recent studies concentrate on the detection and diagnosis of ADS faults using model-based approaches [4]. The challenges of applying model-based approaches to detect and diagnose ADS faults are model uncertainties and external disturbances (atmospheric turbulence). To manage model uncertainties, various approaches, such as H-infinity filters [10], [11], sliding mode observers [12], [13], and observer-based approaches [14], have been proposed. Observers are usually designed based on linear time-invariant systems, whereas the aircraft dynamic model is time-varying. Therefore, linear parameter-varying (LPV) systems must be designed. Alwi and Edwards [15], Varga *et al.* [5], Chen *et al.* [16], and Efimov *et al.* [17] all designed LPV aircraft models for fault detection. Alternatively, the kinematic model of the aircraft can be used to resolve the issue of model uncertainties [6], [18]. The kinematic model uses the measured forces to avoid calculation using uncertain aerodynamic parameters. The kinematic model is valid within the entire flight envelope, and therefore, an LPV system does not need to be designed. However, none of these approaches have considered the effects of atmospheric turbulence.

Validation of sensor fault detection and diagnosis (FDD) approaches on large commercial aircraft is challenging. To bridge the gap between academic research and industrial practice, several research groups have validated their approaches using real flight data [11], [19], [20]. The industry has also implemented fault diagnosis approaches on their aircraft [21], [22]. Lu *et al.* [23] managed to validate inertial measurement unit FDD using real flight data in the presence of turbulence. However, validation of ADS FDD in the presence of atmospheric turbulence has not been achieved using real flight data.

This brief addresses the aircraft ADS FDD in the presence of atmospheric turbulence. The effects of the atmospheric turbulence are analyzed, and a novel kinematic model is proposed, which incorporates the effects of the turbulence. The double-model adaptive estimation (DMAE) approach is extended to address the situation when the effects of faults and external disturbances are coupled. The proposed approach is extensively validated under various turbulence situations using simulated and real flight test data.

The main contributions of this brief are as follows.

1) A novel aircraft kinematic model that explicitly takes the effects of turbulence into consideration is proposed.
2) A covariance adaptation technique is proposed for the DMAE approach to manage ADS FDD in the presence of atmospheric turbulence.
3) The proposed approach is validated using real flight test data in the presence of atmospheric turbulence for the first time.

Manuscript received May 21, 2020; revised July 31, 2020; accepted September 17, 2020. Date of publication October 2, 2020; date of current version August 5, 2021. Manuscript received in final form September 18, 2020. This work was supported by the Foundation Committee of Basic and Applied Basic Research of Guangdong Province under Fund 2019A1515011252. Recommended by Associate Editor M. Abbaszadeh. *(Corresponding author: Peng Lu.)*

Peng Lu is with the Department of Mechanical Engineering, The University of Hong Kong, Hong Kong, China (e-mail: lupeng@hku.hk).

Erik-Jan van Kampen, Coen de Visser, and Qiping Chu are with the Control and Simulation Division, Faculty of Aerospace Engineering, Delft University of Technology, 2629HS Delft, The Netherlands (e-mail: e.vankampen@tudelft.nl; c.c.devisser@tudelft.nl; q.chu@tudelft.nl).

Color versions of one or more of the figures in this article are available online at https://ieeexplore.ieee.org.

Digital Object Identifier 10.1109/TCST.2020.3025725

II. Novel Aircraft Kinematic Model Incorporating the Effects of Atmospheric Turbulence

Van Eykeren and Chu [18] and Lu *et al.* [6] proposed to use an aircraft kinematic model to resolve aircraft ADS FDD. However, their model does not take the effects of atmospheric turbulence into account. This section will present a novel kinematic model that will be used for ADS FDD in the presence of turbulence.

The dynamics of the ground velocity of the aircraft expressed in the body frame V_g^B are as follows:

$$\dot{V}_g^B = A + T_{be}g - \omega \times V_g^B \tag{1}$$

where $A = [A_x, A_y, A_z]^T$ denotes the specific force vector, $\omega = [p, q, r]^T$ is the angular velocity vector, T_{be} is the transformation matrix from inertial frame to body frame, and $g = [0, 0, 9.81]^T$.

Since $V_g^B = V_a^B + V_w^B$, where $V_a^B = [u_a, v_a, w_a]^T$ and $V_w^B = [u_w, v_w, w_w]^T$ are the air velocity and wind velocity vectors, respectively, the air velocity dynamics can be derived as follows:

$$\dot{V}_a^B = A + T_{be}g - \omega \times V_a^B - \left(\dot{V}_w^B + \omega \times V_w^B\right). \tag{2}$$

The effects of the atmospheric turbulence are denoted by

$$d = -\dot{V}_w^B - \omega \times V_w^B := [d_u, d_v, d_w]^T. \tag{3}$$

It is seen that the turbulence has a significant effect on the airspeed dynamics. Since the air velocity vector is not directly measurable, we will reformulate (2) using the true airspeed V, angle of attack α, and angle of sideslip β that are directly measured by the ADSs.

The dynamics of $[V, \alpha, \beta]^T$ can be obtained using those of $[u_a, v_a, w_a]^T$ by the following relationships:

$$\dot{V} = \dot{u}_a c\alpha c\beta + \dot{v}_a s\beta + \dot{w}_a s\alpha c\beta \tag{4}$$

$$\dot{\alpha} = (\dot{w}_a c\alpha - \dot{u}_a s\alpha)/(Vc\beta) \tag{5}$$

$$\dot{\beta} = (-\dot{u}_a c\alpha s\beta + \dot{v}_a c\beta - \dot{w}_a s\alpha s\beta)/V \tag{6}$$

where $c\bullet$ denotes $\cos\bullet$ and $s\bullet$ denotes $\sin\bullet$ for simplicity.

Therefore, the following dynamics of $[V, \alpha, \beta]^T$ are obtained:

$$\begin{aligned}\dot{V} = {} & (A_x - gs\theta + rv_a - qw_a + d_u)c\alpha c\beta \\ & + (A_y + gs\phi c\theta + pw_a - ru_a + d_v)s\beta \\ & + (A_z + gc\phi c\theta + qu_a - pv_a + d_w)s\alpha c\beta\end{aligned} \tag{7}$$

$$\begin{aligned}\dot{\alpha} = {} & [(A_z + gc\phi c\theta + qu_a - pv_a + d_w)c\alpha \\ & - (A_x - gs\theta + rv_a - qw_a + d_u)s\alpha]/(Vc\beta)\end{aligned} \tag{8}$$

$$\begin{aligned}\dot{\beta} = {} & [-(A_x - gs\theta + rv_a - qw_a + d_u)c\alpha s\beta \\ & + (A_y + gs\phi c\theta + pw_a - ru_a + d_v)c\beta \\ & - (A_z + gc\phi c\theta + qu_a - pv_a + d_w)s\alpha s\beta]/V\end{aligned} \tag{9}$$

where d_u, d_v, and d_w are defined in (3), and ϕ, θ, and ψ are the roll, pitch, and yaw angles. Using the following relationships:

$$u_a = Vc\alpha c\beta \tag{10}$$

$$v_a = Vs\beta \tag{11}$$

$$w_a = Vs\alpha c\beta. \tag{12}$$

Equations (7)–(9) can be simplified into

$$\begin{aligned}\dot{V} = {} & (A_x - gs\theta + d_u)c\alpha c\beta + (A_y + gs\phi c\theta + d_v)s\beta \\ & + (A_z + gc\phi c\theta + d_w)s\alpha c\beta\end{aligned} \tag{13}$$

$$\begin{aligned}\dot{\alpha} = {} & [(A_z + gc\phi c\theta + d_w)c\alpha - (A_x - gs\theta + d_u)s\alpha]/Vc\beta \\ & + q - (pc\alpha + rs\alpha)t\beta\end{aligned} \tag{14}$$

$$\begin{aligned}\dot{\beta} = {} & [-(A_x - gs\theta + d_u)c\alpha s\beta + (A_y + gs\phi c\theta + d_v)c\beta \\ & - (A_z + gc\phi c\theta + d_w)s\alpha s\beta]/V + ps\alpha - rc\alpha\end{aligned} \tag{15}$$

where $t\bullet$ denotes $\tan\bullet$ for simplicity. Since the above equations involve the Euler angles, the following kinematics are also necessary to obtain the state estimates:

$$\dot{\phi} = p + qs\phi t\theta + rc\phi t\theta \tag{16}$$

$$\dot{\theta} = qc\phi - rs\phi \tag{17}$$

$$\dot{\psi} = q\frac{s\phi}{c\theta} + r\frac{c\phi}{c\theta}. \tag{18}$$

Equations (13)–(18) are the proposed novel kinematic model. However, for aircraft ADS FDD, we still need to formulate the process model and measurement model. In the kinematic model, A_x, A_y, A_z, p, q, and r are obtained using the measurements from the inertial measurement unit and serve as the input. By this means, uncertain aerodynamic parameters are not required. Furthermore, the kinematic model is valid during the entire flight envelope, and there is no need to design an LPV system.

Defining $u^0 = [A_x, A_y, A_z, p, q, r]^T$, u^0 can be obtained from the measurements of the inertial measurement unit defined as

$$u = [A_{xm}, A_{ym}, A_{zm}, p_m, q_m, r_m]^T \tag{19}$$

$$\begin{aligned} & = [A_x, A_y, A_z, p, q, r]^T + [w_{A_x}, w_{A_y}, w_{A_z}, w_p, w_q, w_r]^T \\ & := u^0 + w\end{aligned} \tag{20}$$

where $w = [w_{A_x}, w_{A_y}, w_{A_z}, w_p, w_q, w_r]^T$ denotes the noise in the inertial measurement unit with covariance matrix $Q = E[ww^T]$. Now, we are ready to rewrite (13)–(18) into the following process model form:

$$\dot{x} = \bar{f}(x, u) + G(x)w + E(x)d \tag{21}$$

where $x = [V, \alpha, \beta, \phi, \theta, \psi]^T \in \mathbb{R}^n$ with $n = 6$, and u and w are defined in (19) and (20) respectively. d, defined in (3), will be treated as unknown disturbances. The nonlinear function $\bar{f}$ is given as follows:

$$\begin{cases} (A_{xm} - gs\theta)c\alpha c\beta + (A_{ym} + gs\phi c\theta)s\beta \\ \quad + (A_{zm} + gc\phi c\theta)s\alpha c\beta \\ [(A_{zm} + gc\phi c\theta)c\alpha - (A_{xm} - gs\theta)s\alpha]/Vc\beta + q_m \\ \quad - (p_m c\alpha + r_m s\alpha)t\beta \\ [(gs\theta - A_{xm})c\alpha s\beta + (A_{ym} + gs\phi c\theta)c\beta \\ \quad - (A_{zm} + gc\phi c\theta)s\alpha s\beta]/V + p_m s\alpha - r_m c\alpha \\ p_m + q_m s\phi t\theta + r_m c\phi t\theta \\ q_m c\phi - r_m s\phi \\ q_m s\phi/c\theta + r_m c\phi/c\theta \end{cases}$$

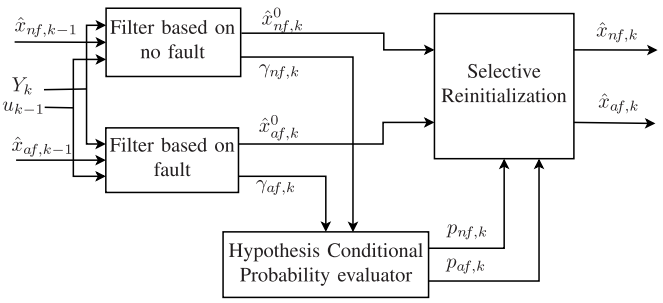

Fig. 1. Block diagram of the DMAE approach at time step k.

The noise and turbulence distribution matrices are derived as

$$G(x) = \begin{bmatrix} -c\alpha c\beta & -s\beta & -s\alpha c\beta & 0 & 0 & 0 \\ \frac{s\alpha}{Vc\beta} & 0 & \frac{-c\alpha}{Vc\beta} & c\alpha t\beta & -1 & s\alpha t\beta \\ \frac{c\alpha s\beta}{V} & \frac{-c\beta}{V} & \frac{s\alpha s\beta}{V} & -s\alpha & 0 & c\alpha \\ 0 & 0 & 0 & -1 & -s\phi t\theta & -c\phi t\theta \\ 0 & 0 & 0 & 0 & -c\phi & s\phi \\ 0 & 0 & 0 & 0 & \frac{-s\phi}{c\theta} & \frac{-c\phi}{c\theta} \end{bmatrix}$$

$$E(x) = \begin{bmatrix} c\alpha c\beta & s\beta & s\alpha c\beta \\ -\frac{s\alpha}{Vc\beta} & 0 & \frac{c\alpha}{Vc\beta} \\ -\frac{c\alpha s\beta}{V} & \frac{c\beta}{V} & -\frac{s\alpha s\beta}{V} \\ 0 & 0 & 0 \\ 0 & 0 & 0 \\ 0 & 0 & 0. \end{bmatrix}$$

The measurement model for the ADS FDD is

$$y = x + Ff + \nu \tag{22}$$

where $y = [V_m, \alpha_m, \beta_m, \phi_m, \theta_m, \psi_m]^T \in \mathbb{R}^m$ with $m = 6$ is the measurement vector, $f = [f_V, f_\alpha, f_\beta]^T \in \mathbb{R}^{n_f}$ with $n_f = 3$ is the ADS fault vector, $\nu = [\nu_V, \nu_\alpha, \nu_\beta, \nu_\phi, \nu_\theta, \nu_\psi]^T$ is the output sensor noise vector with covariance $R = E[\nu\nu^T]$, and $F = [I_{3\times3}, O_{3\times3}]^T$ is the ADS fault distribution matrix.

In summary, (21) and (22) are the novel kinematic model that will be used to detect and diagnose ADS faults. It is observed from these equations that the effects of the ADS faults and atmospheric turbulence are coupled, and the existence condition of disturbance decoupled observers, unknown input observers, or Kalman filters is not satisfied [24], [25]. This poses a significant challenge to ADS FDD in the presence of atmospheric turbulence.

III. Extended Double-Model Adaptive Estimation for FDD in the Presence of Disturbances

A. Design of the DMAE for ADS FDD

The DMAE approach is a framework, which runs two Kalman filters in parallel: a no-fault (fault-free) filter and an augmented fault filter [6]. These two filters are based on two modes of the system: fault-free ($f = 0$) and faulty ($f \neq 0$). Let index i number the two filters where $i = 1$ means the fault-free filter and $i = 2$ denotes the augmented fault filter. The block diagram is shown in Fig. 1. It is seen that both filters use the same measurement history vector $Y_k = [y_1^T, y_2^T, \ldots, y_k^T]^T$ and the input vector u_{k-1}, while each hypothesizes a different fault scenario (fault-free or faulty).

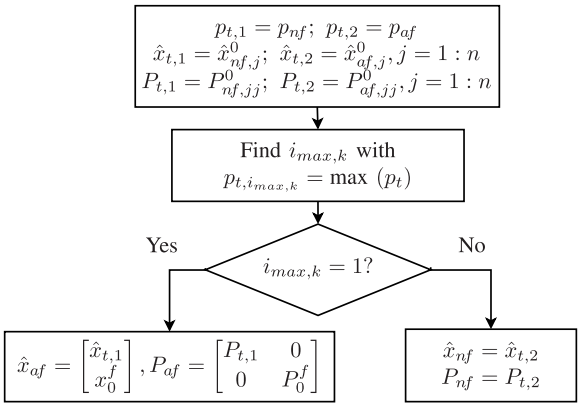

Fig. 2. Flowchart of the selective reinitialization performed by the DMAE.

The state vectors of the no-fault filter $x_{nf} \in \mathbb{R}^n$ and fault filter $x_{af} \in \mathbb{R}^{n+n_f}$ are as follows:

$$x_{nf} = x, \quad x_{af} = \begin{bmatrix} x \\ f \end{bmatrix} \tag{23}$$

where x is defined in (21). Since the no-fault filter assumes that $f = 0$, its measurement model reduces to

$$y = x + \nu = H_{nf}x_{nf} + \nu \tag{24}$$

where $H_{nf} = I_{6\times6}$. The measurement model for the augmented fault filter is

$$y = x + Ff + \nu = H_{af}x_{af} + \nu \tag{25}$$

where $H_{af} = [I_{6\times6}, F]$.

Both filters will generate a state estimate $\hat{x}^0_{i,k}$ and an innovation $\gamma_{i,k}$ at time step k (see the Appendix for the details). The filter that produces the most well-behaved innovation contains the model that best matches the true fault scenario. A hypothesis test will be performed using the innovation $\gamma_{i,k}$ and the innovation covariance matrix $C_{i,k}$ of the filters to assign a conditional probability to both filters.

Let a denote the parameter that specifies a fault scenario, namely $a \in \{a_1, a_2\}$, where a_1 and a_2 denote no-fault and fault scenario, respectively. Define the hypothesis conditional probability $p_{i,k}$ as the probability that a is assigned a_i for $i = 1, 2$, conditioned on the measurement history up to time step k as follows:

$$p_{i,k} = \Pr[a = a_i | Y(k) = Y_k], \quad i = 1, 2. \tag{26}$$

The conditional probability of the two filters can be computed recursively as in [25].

To increase the robustness of the DMAE with respect to model uncertainties and disturbances, a selective reinitialization [25] is performed. The flowchart is presented in Fig. 2. Superscript "0" denotes the variables before the reinitialization. $\hat{x}_t$ contains the first n elements of $\hat{x}^0_{\rm nf}$ and $\hat{x}^0_{\rm af}$. P_t contains the first n rows and n columns of $P_{\rm nf}$ and $P_{\rm af}$. $i_{{\rm max},k}$ denotes the index of the filter with the larger conditional

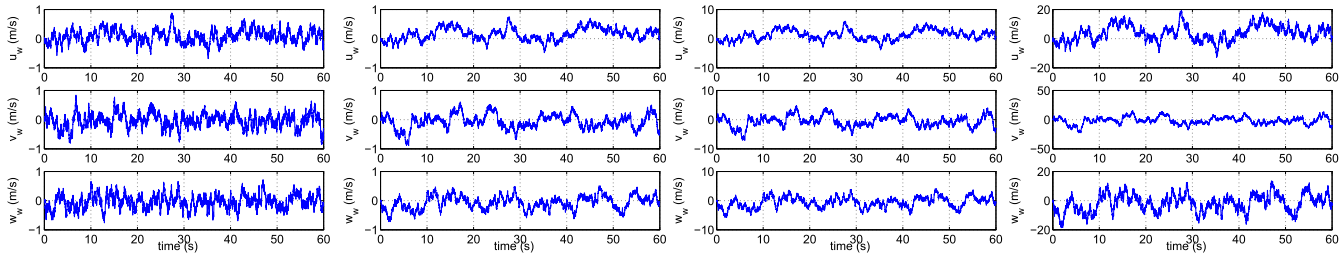

Fig. 3. u_w, v_w, and w_w for the four simulated turbulence scenarios. Note the differences in magnitudes. (a) u_w, v_w, and w_w for case 1. (b) u_w, v_w, and w_w for case 2. (c) u_w, v_w, and w_w for case 3. (d) u_w, v_w, and w_w for case 4.

probability. The principle is to reinitialize the state estimation and covariance matrix of the filter with the lower conditional probability using those of the filter with a higher conditional probability. x_0^f and P_0^f are the reinitialization parameters. Note that the two filters have different dimensions of state vectors and covariance matrices.

A fault is detected if $p_{\text{af}} > p_{\text{nf}}$. The fault estimate $\hat{f}_k$ is obtained using the augmented fault filter. The probability-weighted fault estimate $\hat{f}_k^w$ is computed by

$$\hat{f}_k^w = \hat{f}_k p_{af,k}. \tag{27}$$

B. Extension of the DMAE With Covariance Adaptation for ADS FDD in the Presence of Atmospheric Turbulence

Both filters of the DMAE are designed based on the unscented Kalman filter (UKF) since the kinematic model is nonlinear. The specific design steps are included in the Appendix. It is seen from (21) and (22) that faults and disturbances have coupled effects, and the existence condition of disturbance observers or unknown input observers or Kalman filters is not satisfied. Consequently, this poses a significant challenge for ADS FDD in case of turbulence. This section will extend the DMAE such that it can address fault detection even in the presence of atmospheric turbulence.

Since d is unknown in (21), it is difficult for the UKF to obtain an unbiased estimate of x. If d is treated as a stochastic process driven by white noise with covariance matrix Q_d, then the UKF can yield the unbiased minimum variance estimate of x. However, the optimality of the estimate can be compromised by a poor choice of Q_d. Moreover, the dynamics of atmospheric turbulence are changing significantly. Thus, it is unreasonable to choose a fixed Q_d. In this section, we will present a method that can adaptively update Q_d to achieve unbiased estimates of x. Lu *et al.* [25] also proposed an adaptive method to tune the Q_d. However, their approach is based on a linear discrete-time system and is not directly applicable to the nonlinear system considered in this brief.

The fault is modeled as a stochastic process $\dot{f} = w_f$ with covariance $Q_f = E[w_f w_f^T]$. The innovation of the augmented fault filter at time step k is given as follows:

$$\gamma_{af,k} = y_k - H_{af,k}\hat{x}_{af,k|k-1} \tag{28}$$

$$= H_{af,k}x_{af,k} + v_k - H_{af,k}\hat{x}_{af,k|k-1}. \tag{29}$$

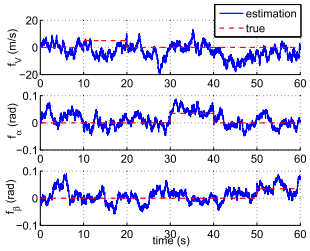

Fig. 4. Fault estimation using the ATSUKF.

The theoretical innovation covariance is computed as follows:

$$C_{af,k} = E\{\gamma_{af,k}\gamma_{af,k}^T\} \tag{30}$$

$$= H_{af,k}P_{af,k|k-1}H_{af,k}^T + R_k \tag{31}$$

$$= H_{af,k}\left(P_{af,k|k-1}^* + Q_{af,k-1}\Delta t\right)H_{af,k}^T + R_k \tag{32}$$

where $\Delta t = t_k - t_{k-1}$, $P_{af,k|k-1}^* = \sum_{i=0}^{2(n+n_f)} W_i^{(c)}[\mathcal{X}_{af,i,k|k-1}^* - \hat{x}_{af,k|k-1}][\mathcal{X}_{af,i,k|k-1}^* - \hat{x}_{af,k|k-1}]^T$ with $\mathcal{X}_{af,i,k|k-1}^*$ computed similarly as in (39). $Q_{af,k-1}$ is defined as follows:

$$\begin{bmatrix} G_{k-1}Q_{k-1}G_{k-1}^T + E_{k-1}Q_{d,k-1}E_{k-1}^T & O \\ O & Q_{f,k-1} \end{bmatrix}.$$

The innovation covariance can be also approximated using the innovation sequence as follows:

$$\hat{C}_{af,k} = \sum_{j=k-N+1}^{k} \gamma_{af,j}\gamma_{af,j}^T / N. \tag{33}$$

Comparing (32) and (33) while neglecting the terms with small magnitudes, Q_d can be estimated using the following:

$$E_{k-1}Q_{d,k-1}E_{k-1}^T\Delta t = \hat{C}_{af,k} - G_{k-1}Q_{k-1}G_{k-1}^T\Delta t - F_k Q_{f,k-1}F_k^T\Delta t - R_k. \tag{34}$$

As E_{k-1} is not invertible, Q_d cannot be directly solved from above. However, it is not necessary to solve Q_d since we only need to compute $E_{k-1}Q_{d,k-1}E_{k-1}^T\Delta t$ in (41).

Define Q_d^0 as follows:

$$\hat{C}_{af,k} - G_{k-1}Q_{k-1}G_{k-1}^T\Delta t - F_k Q_{f,k-1}F_k^T\Delta t - R_k.$$

Then, we can approximate $E_{k-1}Q_{d,k-1}E_{k-1}^T\Delta t$ using the main diagonal elements of Q_d^0. To preserve the properties of

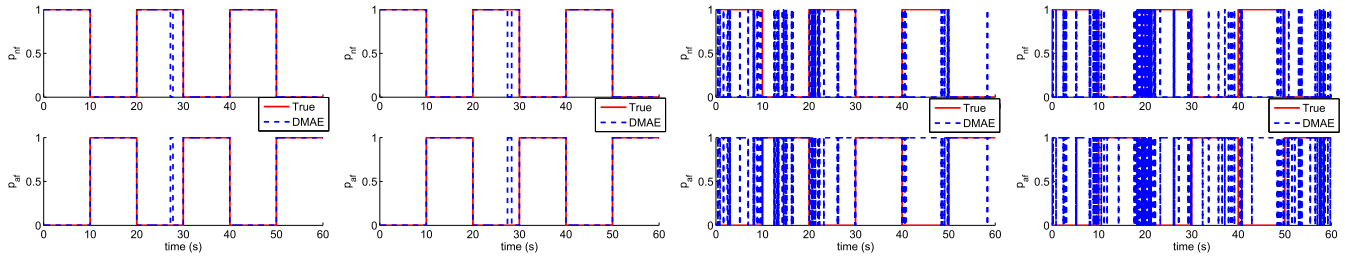

Fig. 5. p_{nf} and p_{af} using the DMAE without covariance adaptation for the four simulated turbulence scenarios. (a) p_{nf} and p_{af} for case 1. (b) p_{nf} and p_{af} for case 2. (c) p_{nf} and p_{af} for case 3. (d) p_{nf} and p_{af} for case 4.

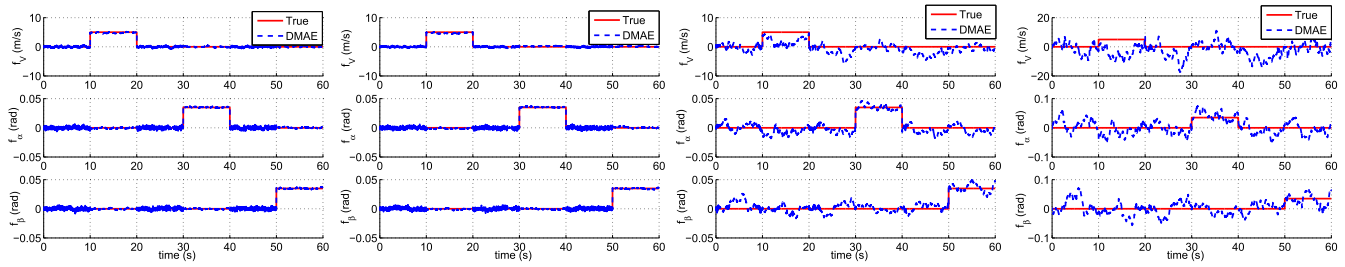

Fig. 6. Fault estimation using the DMAE without covariance adaptation for the four simulated turbulence scenarios. (a) Fault estimation for case 1. (b) Fault estimation for case 2. (c) Fault estimation for case 3. (d) Fault estimation for case 4.

a variance, the following is used:

$$E_{k-1}Q_{d,k-1}E_{k-1}^{T}\Delta t = \operatorname{diag}\big[\max\big(Q_{d,11}^{0},0\big),\max\big(Q_{d,22}^{0},0\big),\max\big(Q_{d,33}^{0},0\big),\max\big(Q_{d,44}^{0},0\big),\max\big(Q_{d,55}^{0},0\big),\max\big(Q_{d,66}^{0},0\big)\big]$$

where $Q_{d,jj}^{0}$ denotes the jth row, jth column element of Q_{d}^{0}, and $\max(Q_{d,11}^{0},0)$ denotes the maximum value between $Q_{d,11}^{0}$ and 0. In addition, note that the last three rows of E_{k-1} are zero. Therefore, $E_{k-1}Q_{d,k-1}E_{k-1}^{T}\Delta t$ is approximated by

$$\operatorname{diag}\big[\max\big(Q_{d,11}^{0},0\big),\max\big(Q_{d,22}^{0},0\big),\max\big(Q_{d,33}^{0},0\big),0,0,0\big].$$

IV. Simulation Validation

A. Turbulence Scenarios

The turbulence velocities ($V_{w}^{B}=[u_{w},v_{w},w_{w}]^{T}$) are generated using the Dryden model [26], the power spectral density functions of which are given as follows:

$$\Phi_{u}(\omega_{o})=\frac{2\sigma_{u}^{2}L_{u}}{\pi V}\frac{1}{1+(L_{u}\omega_{o}/V)^{2}} \tag{35}$$

$$\Phi_{v}(\omega_{o})=\frac{\sigma_{v}^{2}L_{v}}{\pi V}\frac{1+3(L_{v}\omega_{o}/V)^{2}}{(1+(L_{v}\omega_{o}/V)^{2})^{2}} \tag{36}$$

$$\Phi_{w}(\omega_{o})=\frac{\sigma_{w}^{2}L_{w}}{\pi V}\frac{1+3(L_{w}\omega_{o}/V)^{2}}{(1+(L_{w}\omega_{o}/V)^{2})^{2}} \tag{37}$$

where V is the true airspeed and ω_{o} is the observed angular frequency. L_{u}, L_{v}, and L_{w} are the scale lengths and σ_{u}, σ_{v}, and σ_{w} are the intensities of the turbulence.

It is assumed that the turbulence field is isotropic [26]; therefore, $L_{u}=L_{v}=L_{w}$ and $\sigma_{u}=\sigma_{v}=\sigma_{w}$.

TABLE I

Scenarios With Different Scale Lengths and Intensities

Variables	Case 1	Case 2	Case 3	Case 4
L_{u}, L_{v}, L_{w} [m]	150	530	530	530
σ_{u}, σ_{v}, σ_{w} [m/s]	0.25	0.25	2	6.4

Four turbulence scenarios with various scale lengths and intensities, as presented in Table I, are generated for validation.

The turbulence data are recursively generated using differential equations. Especially, u_{w} is generated using the following differential equation:

$$\dot{u}_{w}=-u_{w}\frac{V}{L_{u}}+\sigma_{u}w'\sqrt{\frac{2V}{\pi L_{u}}}$$

where $w'\sim N(0,1)$. v_{w} can be generated using the following second-order differential equation [26]:

$$\begin{bmatrix}\dot{v}_{w}\\ \dot{v}_{w}^{*}\end{bmatrix}=\begin{bmatrix}0 & 1\\ -\dfrac{V^{2}}{L_{v}^{2}} & -2\dfrac{V}{L_{v}}\end{bmatrix}\begin{bmatrix}v_{w}\\ v_{w}^{*}\end{bmatrix}+\begin{bmatrix}\sigma_{v}\sqrt{\dfrac{3V}{\pi L_{v}}}\\ (1-2\sqrt{3})\sigma_{v}\sqrt{\dfrac{V^{3}}{\pi L_{v}^{3}}}\end{bmatrix}w''$$

where $w''\sim N(0,1)$ and v_{w}^{*} is an intermediate variable. w_{w} can be generated as similar as v_{w}.

The generated u_{w}, v_{w}, and w_{w} of the four cases are shown in Fig. 3. Note that the scale length and intensity of case 4 are close to those of a thunderstorm [26].

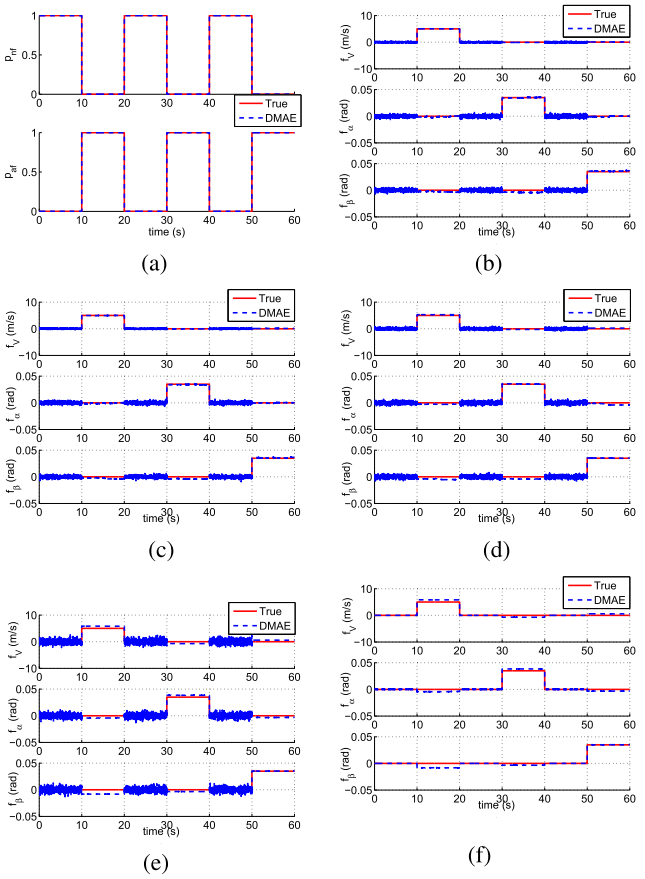

Fig. 7. Results using the DMAE with covariance adaptation for four simulated turbulence scenarios. (a) p_{nf} and p_{af} for four cases. (b) Fault estimation for case 1. (c) Fault estimation for case 2. (d) Fault estimation for case 3. (e) Fault estimation for case 4. (f) Weighted fault estimation for case 4.

B. ADS FDD Validation in the Presence of Turbulence

The novel DMAE with covariance adaptation will be validated using the four different turbulence scenarios given in Table I. For comparison, existing approaches and the DMAE without covariance adaptation will also be validated. The ADS faults are denoted by the red solid lines in Fig. 6. The source code is available at.[1]

Existing disturbance observers or unknown input observers cannot decouple the faults from the turbulence since the existence condition to design a decouple observer is not satisfied [25]. For example, the unknown input observer [27] diverges due to the fact that a decoupled unknown input observer cannot be designed. Unknown input Kalman filters also cannot decouple the faults from the turbulence. For example, the fault estimation using the adaptive three-step unscented Kalman filter [20] is shown in Fig. 4. It is seen that the faults and turbulence are coupled, and it is difficult to distinguish the faults from the results. Results using other methods are similar and are omitted.

The fault detection using the DMAE without covariance adaptation is shown in Fig. 5. It is seen that the false alarm rate increases as the turbulence intensity increases. The estimated faults ($\hat{f} = [\hat{f}_V, \hat{f}_\alpha, \hat{f}_\beta]^T$) are presented in Fig. 6. It is seen that the fault estimation is coupled with the turbulence. As the intensity of the turbulence increases, it is difficult to distinguish the fault from the turbulence.

[1] https://github.com/lplp8899/ADS_FDD_Turbulence

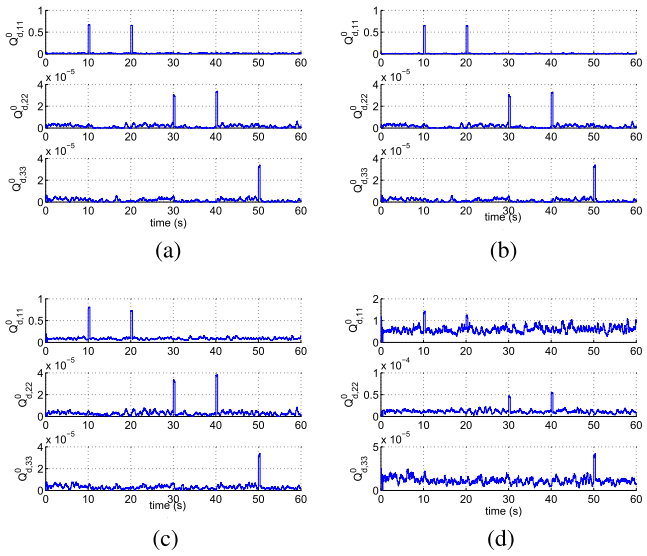

Fig. 8. Main diagonal elements of Q_d^0 for simulated turbulence cases. (a) Q_d^0 for turbulence case 1. (b) Q_d^0 for turbulence case 2. (c) Q_d^0 for turbulence case 3. (d) Q_d^0 for turbulence case 4.

On the contrary, the FDD using the proposed DMAE with covariance adaptation can successfully decouple the fault from the turbulence even when the intensity of the turbulence increases. The fault detection using the proposed approach for four turbulence scenarios is the same and is shown in Fig. 7(a). It is seen that there are no false alarms. The fault estimates for the four scenarios are shown in Fig. 7(b)–(e), respectively. As can be seen, all faults are estimated and decoupled from the turbulence.

The fault estimates when there are no faults (during $0 < t < 10$ s, $20 < t < 30$ s, and $40 < t < 50$ s) become noisier as the turbulence intensity increases. However, the fault shape can be recovered readily using the probability-weighted fault estimates denoted by $\hat{f}_w$. For example, the probability-weighted fault estimates for case 4 are shown in Fig. 7(f).

The first three main diagonal elements of Q_d^0 for the four cases are shown in Fig. 8(a)–(d), respectively. It is seen that the magnitude of Q_d^0 will increase as the intensity increases. Moreover, Q_d^0 increases significantly when a fault occurs.

V. Real Flight Test Data Verification

To bridge the gap between academic research and real practice, we performed several flight tests to collect flight data when the aircraft is flying in turbulence. The Cessna Citation II aircraft, which is owned by the Delft University of Technology and the Dutch Aerospace Lab, is used.

Real flight data when the aircraft [shown in Fig. 9(a)] was experiencing atmospheric turbulence are shown in Fig. 9(b). The turbulence occurred at around $t > 20$ s when the aircraft is descending. It is seen that the vertical acceleration A_z and α oscillate significantly due to the occurrence of the turbulence.

The DMAE with and without covariance adaptation will be validated using these flight data. The original real data do

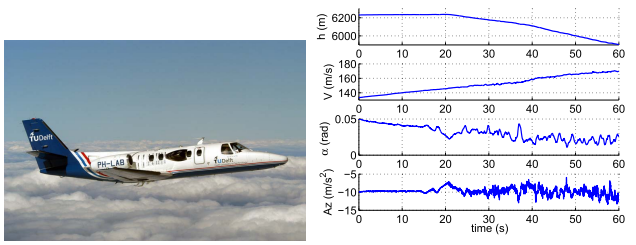

(a) (b)

Fig. 9. Real flight tests performed using the Cessna Citation II aircraft. (a) Cessna Citation II aircraft for the real flight tests. (b) Response of the aircraft during the presence of turbulence.

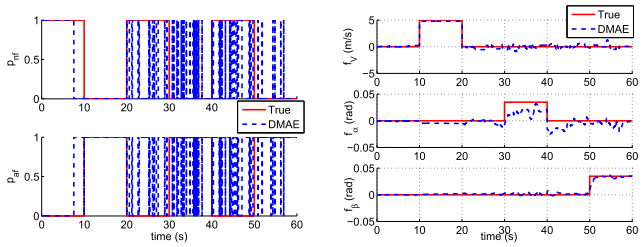

(a) (b)

Fig. 10. ADS FDD using the DMAE without covariance adaptation in the presence of real atmospheric turbulence. (a) p_{nf} and p_{af} for consecutive ADS FDD. (b) Fault estimation for consecutive ADS FDD.

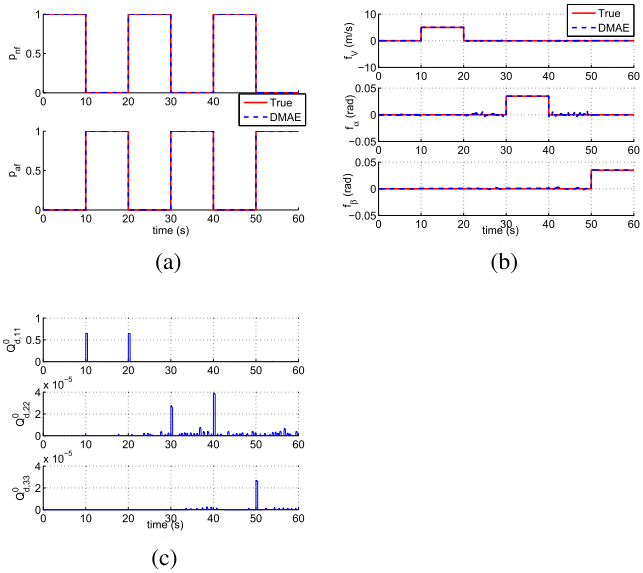

(a) (b) (c)

Fig. 11. Consecutive ADS FDD using the DMAE with covariance adaptation in the presence of real atmospheric turbulence. (a) p_{nf} and p_{af} for consecutive ADS FDD. (b) Fault estimation for consecutive ADS FDD. (c) Q_d^0 for consecutive faults.

not contain ADS faults, and we add the same faults as in the simulation to the real flight data. It should be noted that injecting ADS faults online to manned aircraft is extremely dangerous as the air data information is critical to flight safety. However, it was demonstrated in [23] that if states and faults are estimated in an unbiased sense, then the difference of performing fault diagnosis online and offline using the kinematic model is negligible.

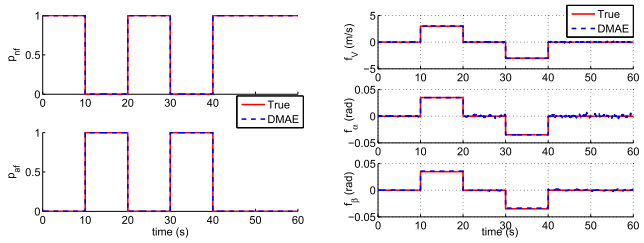

(a) (b)

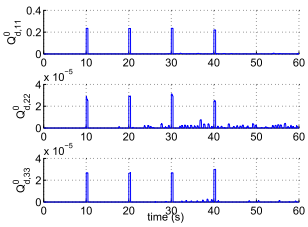

(c)

Fig. 12. Simultaneous ADS FDD using the DMAE with covariance adaptation in the presence of real turbulence. (a) p_{nf} and p_{af} for simultaneous ADS FDD. (b) Fault estimation for simultaneous ADS FDD. (c) Q_d^0 for simultaneous faults.

The fault detection using the DMAE without covariance adaptation is shown in Fig. 10(a). Many false alarms appear after $t > 20$ s, which is the occurrence time of the turbulence. The fault estimation is also significantly affected by the turbulence, as shown in Fig. 10(b).

The fault detection using the proposed DMAE with covariance adaptation is shown in Fig. 11(a). All faults are detected, and no false alarm is observed, which demonstrates the fault detection performance of the proposed approach. The fault estimates are shown in Fig. 11(b). All faults are estimated and decoupled from the turbulence. The first three main diagonal elements of Q_d^0 are displayed in Fig. 11(c). The results are similar to those in simulation. The magnitude of Q_d^0 increases when faults occur.

To further demonstrate the performance of the proposed approach, simultaneous faults are also addressed. The detection of simultaneous faults is shown in Fig. 12(a). The estimates of the simultaneous faults are shown in Fig. 12(b). Again, all simultaneous faults are estimated and decoupled from the effect of the turbulence. The first three main diagonal elements of Q_d^0 are displayed in Fig. 12(c). Q_d^0 increases significantly when faults occur or disappear.

VI. Conclusion

This brief addressed the ADS FDD when the aircraft is experiencing turbulence. The proposed double-model adaptive estimation with covariance adaptation can decouple and estimate faults from turbulence.

To bridge the gap between academic research and industrial practice, the proposed approach is validated using real flight test data when the aircraft is flying in atmospheric turbulence. An interesting future work would be to generate faults during the flight. However, this is particularly dangerous as the air data information is critical to flight safety and the validation on unmanned aerial vehicles is recommended. Due to the

challenge that the effects of faults and turbulence are coupled, currently, the approach can only address bias faults. Addressing any types of faults in the presence of turbulence is still under investigation.

APPENDIX

Both the no-fault filter and augmented fault filter estimate the states using the UKF. In this appendix, we use the no-fault filter as the example. For readability, subscript "nf" is omitted, and all variables in this appendix refer to the no-fault filter. Given state estimates $\hat{x}_{k-1}$ and error covariance matrix P_{k-1} at time step $k-1$, we can compute sigma points as follows:

$$\mathcal{X}_{k-1} = [\hat{x}_{k-1}, \hat{x}_{k-1} - \gamma\sqrt{P_{k-1}}, \hat{x}_{k-1} + \gamma\sqrt{P_{k-1}}] \quad (38)$$

where $\mathcal{X}_{i,k-1}$ are the sigma points of the states x with dimension n (6 for the no-fault filter and 9 for the augmented fault filter) at step $k-1$. $\gamma = (n+\lambda)^{1/2}$. $\lambda = \alpha_0^2(n+\kappa) - n$ with $\kappa = 0$ and $\alpha_0 = 0.8$.

Once the sigma points are obtained, we can derive the state estimation $\hat{x}_k^0$ and its error covariance matrix P_k^0 at time step k using the following time update and measurement update.

1) *Time Update:* Based on the computed sigma points, the predicted mean $\hat{x}_{k|k-1}$ and its error covariance matrix $P_{k|k-1}$ are computed as follows:

$$\mathcal{X}^*_{i,k|k-1} = \mathcal{X}_{i,k-1} + \int_{t_{k-1}}^{t_k} \bar{f}(\mathcal{X}_{i,k-1}, u(\tau))d\tau \quad (39)$$

$$\hat{x}_{k|k-1} = \sum_{i=0}^{2\ n} W_i^{(m)} \mathcal{X}^*_{i,k|k-1} \quad (40)$$

$$P_{k|k-1} = P^*_{k|k-1} + G_{k-1}Q_{k-1}G_{k-1}^T\Delta t + E_{k-1}Q_{d,k-1}E_{k-1}^T\Delta t \quad (41)$$

where $P^*_{k|k-1} = \sum_{i=0}^{2n} W_i^{(c)}[\mathcal{X}^*_{i,k|k-1} - \hat{x}_{k|k-1}][\mathcal{X}^*_{i,k|k-1} - \hat{x}_{k|k-1}]^T$, and $\Delta t = t_k - t_{k-1}$. Q and Q_d are the covariance matrices of w [as defined in (20)] and d [as defined in (3)], respectively. $P_{k|k-1}$ for the fault filter is given in (31). Redraw sigma points as follows [28, p. 233]:

$$\mathcal{X}_{k|k-1} = [\hat{x}_{k|k-1}, \hat{x}_{k|k-1} - \gamma\sqrt{P_{k|k-1}}, \hat{x}_{k|k-1} + \gamma\sqrt{P_{k|k-1}}]$$

then

$$\mathcal{Y}_{i,k|k-1} = H_k\mathcal{X}_{i,k|k-1} \quad (42)$$

$$\hat{y}_k = \sum_{i=0}^{2n} W_i^{(m)}\mathcal{Y}_{i,k|k-1} \quad (43)$$

$$P_{xy,k} = \sum_{i=0}^{2n} W_i^{(c)}[\mathcal{X}_{i,k|k-1} - \hat{x}_{k|k-1}][\mathcal{Y}_{i,k|k-1} - \hat{y}_k]^T \quad (44)$$

$$P_{yy,k} = \sum_{i=0}^{2n} W_i^{(c)}[\mathcal{Y}_{i,k|k-1} - \hat{y}_k][\mathcal{Y}_{i,k|k-1} - \hat{y}_k]^T + R \quad (45)$$

where $W_i^{(m)}$ and $W_i^{(c)}$ are the weights associated with the ith point with respect to $\hat{x}_{k-1}$ and P_{k-1} and are calculated according to [29].

2) *Measurement Update:*

$$K_k = P_{xy,k}P_{yy,k}^{-1} \quad (46)$$

$$\gamma_k = y_k - \hat{y}_k \quad (47)$$

$$\hat{x}_k^0 = \hat{x}_{k|k-1} + K_k\gamma_k \quad (48)$$

$$P_k^0 = P_{k|k-1} - K_kP_{yy,k}K_k^T \quad (49)$$

where y_k is the measurement vector. γ_k is the innovation, and K_k is the Kalman gain of the UKF.

$\hat{x}_k^0$ and P_k^0 are the state estimate and error covariance matrix at time step k. They are used by the selective reinitialization block shown in Figs. 1 and 2 to obtain $\hat{x}_k$ and P_k for the no-fault filter. Then, $\hat{x}_k$ and P_k are regarded as the prior knowledge for step $k+1$, as denoted in (38).

REFERENCES

[1] BEA, "Final report on the accident on 1st Jun. 2009 to the Airbus A330-203 registered F-GZCP operated by air France flight AF 447 rio de Janeiro Paris," Bureau d'Enquêtes et d'Analyses pour la sécurité de l'aviation civile, Paris, France, Tech. Rep. f-cp090601, Jun. 2012.

[2] F. L. Carpenter, "Summary of facts- B2 accident on 23 Feb. 2008," Accident Invest. Board, Latin, Norway, Tech. Rep. S/N 89-0127, 20080223, 2008.

[3] P. Castaldi, W. Geri, M. Bonfè, S. Simani, and M. Benini, "Design of residual generators and adaptive filters for the FDI of aircraft model sensors," *Control Eng. Pract.*, vol. 18, no. 5, pp. 449–459, May 2010.

[4] P. Freeman, P. Seiler, and G. J. Balas, "Air data system fault modeling and detection," *Control Eng. Pract.*, vol. 21, no. 10, pp. 1290–1301, Oct. 2013.

[5] A. Varga, D. Ossmann, and H. Joos, "A fault diagnosis based reconfigurable longitudinal control system for managing loss of air data sensors for a Civil Aircraft," in *Proc. Int. Fed. Autom. Control World Congr.*, Cape Town, South Africa, 2014, pp. 1–5.

[6] P. Lu, L. Van Eykeren, E.-J. van Kampen, C. de Visser, and Q. Chu, "Double-model adaptive fault detection and diagnosis applied to real flight data," *Control Eng. Pract.*, vol. 36, pp. 39–57, Mar. 2015.

[7] Y. Wan, T. Keviczky, and M. Verhaegen, "Robust air data sensor fault diagnosis with enhanced fault sensitivity using moving horizon estimation," in *Proc. Amer. Control Conf. (ACC)*, Jul. 2016, pp. 5969–5975.

[8] J. Ellsworth and S. Whitmore, "Reentry air data for a sub-orbital spacecraft based on X-34 design," in *Proc. 45th AIAA Aerosp. Sci. Meeting Exhibit*, Reno, Nevada Jan. 2007, pp. 1–31.

[9] F. Nebula, R. Palumbo, and G. Morani, "Virtual air data: A fault-tolerant approach against ADS failures," in *Proc. AIAA Infotech Aerospace*, Boston, MA, USA, Aug. 2013, pp. 1–14.

[10] A. Marcos, "Assessment on the ADDSAFE benchmark simulator of an H-$_{infinity}$ fault detection design for aircraft," in *8th IFAC Symp. Fault Detection, Supervision Saf. Tech. Processes*, 2012, pp. 1341–1346.

[11] R. Venkataraman, P. Bauer, P. Seiler, and B. Vanek, "Comparison of fault detection and isolation methods for a small unmanned aircraft," *Control Eng. Pract.*, vol. 84, pp. 365–376, Mar. 2019.

[12] H. Alwi, L. Chen, and C. Edwards, "Reconstruction of Simultaneous Actuator and Sensor Faults for the RECONFIGURE Benchmark Using a Sliding Mode Observer," in *The Int. Fed. Autom. Control World Congr.*, Cape Town, South Africa, 2014, pp. 3497–3502.

[13] A. F. de Loza, D. Henry, J. Cieslak, A. Zolghadri, and J. Dávila, "Sensor fault diagnosis using a non-homogeneous high-order sliding mode observer with application to a transport aircraft," *IET Control Theory Appl.*, vol. 9, no. 4, pp. 598–607, Feb. 2015.

[14] E. Kiyak, Ö. Çetin, and A. Kahveciolu, "Aircraft sensor fault detection based on unknown input observers," *Aircr. Eng. Aerosp. Technol.*, vol. 80, no. 5, pp. 545–548, Sep. 2008.

[15] H. Alwi and C. Edwards, "Development and application of sliding mode LPV fault reconstruction schemes for the ADDSAFE benchmark," *Control Eng. Pract.*, vol. 31, pp. 148–170, Oct. 2014.

[16] L. Chen, R. Patton, and P. Goupil, "Robust fault estimation using an LPV reference model: ADDSAFE benchmark case study," *Control Eng. Pract.*, no. 2, pp. 194–203, Feb.2020.

[17] D. Efimov, L. Fridman, T. Raïssi, A. Zolghadri, and R. Seydou, "Interval estimation for LPV systems applying high order sliding mode techniques," *Automatica*, vol. 48, no. 9, pp. 2365–2371, Sep. 2012.
[18] L. Van Eykeren and Q. P. Chu, "Sensor fault detection and isolation for aircraft control systems by kinematic relations," *Control Eng. Pract.*, vol. 31, pp. 200–210, Oct. 2014.
[19] D. Berdjag, J. Cieslak, and A. Zolghadri, "Fault diagnosis and monitoring of oscillatory failure case in aircraft inertial system," *Control Eng. Pract.*, vol. 20, no. 12, pp. 1410–1425, Dec. 2012.
[20] P. Lu, L. Van Eykeren, E. van Kampen, C. C. de Visser, and Q. P. Chu, "Adaptive three-step Kalman filter for air data sensor fault detection and diagnosis," *J. Guid., Control, Dyn.*, vol. 39, no. 3, pp. 590–604, Mar. 2016.
[21] P. Goupil, "AIRBUS state of the art and practices on FDI and FTC in flight control system," *Control Eng. Pract.*, vol. 19, no. 6, pp. 524–539, Jun. 2011.
[22] A. Zolghadri, J. Cieslak, D. Efimov, P. Goupil, and R. Dayre, "Practical design considerations for successful industrial application of model-based fault detection techniques to aircraft systems," *Annu. Rev. Control*, vol. 42, pp. 224–231, Oct. 2016.
[23] P. Lu, E.-J. van Kampen, C. de Visser, and Q. Chu, "Nonlinear aircraft sensor fault reconstruction in the presence of disturbances validated by real flight data," *Control Eng. Pract.*, vol. 49, pp. 112–128, Apr. 2016.
[24] F. Ben Hmida, K. Khémiri, J. Ragot, and M. Gossa, "Unbiased minimum-variance filter for state and fault estimation of linear time-varying systems with unknown disturbances," *Math. Problems Eng.*, vol. 2010, pp. 1–17, Dec. 2010.
[25] P. Lu, E.-J. van Kampen, C. C. de Visser, and Q. Chu, "Framework for state and unknown input estimation of linear time-varying systems," *Automatica*, vol. 73, pp. 145–154, Nov. 2016.
[26] D. Mclean, *Automatic Flight Control Systerm*. Englewood Cliffs, NJ, USA: Prentice-Hall, 1990.
[27] M. Saif and Y. Guan, "A new approach to robust fault detection and identification," *IEEE Trans. Aerosp. Electron. Syst.*, vol. 29, no. 3, pp. 685–695, Jul. 1993.
[28] E. A. Wan and R. van der Merwe, *The Unscented Kalman Filter*. Hoboken, NJ, USA: Wiley, 2017, pp. 221–280.
[29] S. J. Julier and J. K. Uhlmann, "Unscented filtering and nonlinear estimation," *Proc. IEEE*, vol. 92, no. 3, pp. 401–422, Mar. 2004.